

Article

Effect of Erosion Behavior of FeO-CaO-SiO₂-MgO-Al₂O₃ Blast Furnace Primary Slag on Al₂O₃ Substrate

Xiangyang Pan, Fengman Shen *, Qiangjian Gao, Xin Jiang and Haiyan Zheng 

School of Metallurgy, Northeastern University, Shenyang 110819, China; 1910547@stu.neu.edu.cn (X.P.); gaoqj@smm.neu.edu.cn (Q.G.); jiangx@smm.neu.edu.cn (X.J.); zhenghy@smm.neu.edu.cn (H.Z.)

* Correspondence: shenfm@mail.neu.edu.cn; Tel.: +86-130-3240-2395

Abstract: Al₂O₃ substrate is widely used as a lining refractory material throughout the blast furnace (BF) process. Accordingly, the erosion of Al₂O₃ refractory by molten slag has a negative influence on the running cost and smooth operation of BFs. The effect of the erosion behavior of BF primary slag containing FeO-CaO-SiO₂-MgO-Al₂O₃ on Al₂O₃ substrate refractory was fundamentally investigated using the high-temperature contact angle method and FactSage thermodynamic software based on the composition of BF primary slag in a typical iron and steel enterprise of China. The results showed that the primary slag mentioned above was easily wetted with Al₂O₃ substrate, and the observed contact angles were 24.5° and 22.0°, when the FeO mass fraction ($w(\text{FeO})$) was maintained at 10% and 15% of the primary slag, respectively. Moreover, the starting melting temperature of the primary slag with high FeO content, of 1263 °C, was lower. The erosion thickness between the slag and Al₂O₃ substrate increased from 19.23 to 23.17 μm as the added $w(\text{FeO})$ increased from 10% to 15%. In addition, it was observed via SEM-EDS analysis that the interface layer was formed, and high-melting-point compounds were generated during the wetting process. This was attributed to the interaction between the molten slag and Al₂O₃ existing in the substrate, which may have inhibited the continuous dissolution of the Al₂O₃ in the substrate into slag. Good surface wettability and the dissolution of the Al₂O₃ substrate refractory into the primary slag of the BF are two dominant factors leading to the erosion of the refractory.

Keywords: Al₂O₃ substrate; $w(\text{FeO})$; line scanning; wettability; erosion thickness



Citation: Pan, X.; Shen, F.; Gao, Q.; Jiang, X.; Zheng, H. Effect of Erosion Behavior of FeO-CaO-SiO₂-MgO-Al₂O₃ Blast Furnace Primary Slag on Al₂O₃ Substrate. *Crystals* **2021**, *11*, 957. <https://doi.org/10.3390/cryst11080957>

Academic Editors: Yufeng Guo, Shuai Wang, Mao Chen, Kexin Jiao, Lingzhi Yang, Feng Chen and Fuqiang Zheng

Received: 21 July 2021

Accepted: 14 August 2021

Published: 16 August 2021

Publisher's Note: MDPI stays neutral with regard to jurisdictional claims in published maps and institutional affiliations.



Copyright: © 2021 by the authors. Licensee MDPI, Basel, Switzerland. This article is an open access article distributed under the terms and conditions of the Creative Commons Attribution (CC BY) license (<https://creativecommons.org/licenses/by/4.0/>).

1. Introduction

In modern BF technology, due to the dual pressures of economic benefits and environmental protection, in addition to the lack of high-quality resources and the need to control operating costs [1], numerous enterprises have been required to increase their use of low-grade iron ore and poor-quality fuel. This inevitably leads to fluctuations in the composition of the BF primary slag, and thus aggravates the erosion by slag of refractory materials [2–4]. To effectively overcome these issues, higher requirements have been proposed for the precise control of the composition of ironmaking slag. The majority of previous studies have focused on the final slag of the CaO-SiO₂-Al₂O₃-MgO slag system. Compared with the final slag, the slag system formed in the lower part of the BF, which is composed of primary slag and bosh slag, has distinct characteristics and different slag behavior [5–9], which has not been fully elucidated to date. In the BF process, it is generally believed that the BF primary slag has more research significance than the final slag [10].

BF primary slag is composed of iron oxide FeO and gangue (mainly SiO₂ and Al₂O₃) in the ore, in addition to artificially added MgO, CaO, and other ingredients. The content of FeO can reach up to 20–30% [11–14]. At the cohesive zone, the BF primary slag produces wetting phenomena with substrate refractory materials, and also erodes the refractory. At elevated temperature conditions, the slag exists in the form of a melt or liquid phase, and the liquid phase slag also reacts with the oxides in the refractory after erosion. Therefore,

the essence of slag erosion is the erosion of the liquid phase slag, that is, the dissolution of refractory into the slag [15,16], and the penetration of the slag into refractory materials. It is well known that slag erosion has a significant impact on the service life of refractory materials and is an important cause of refractory damage. Moreover, the consumption of refractory materials is one of the main costs of BF smelting. Thus, inhibiting the interaction between slag and refractory materials is expected to be an effective means to reduce the consumption of refractory materials [17].

Wettability is related to the ability or propensity of a liquid to spread on a solid surface. The important application of wettability and its significant economic benefits have prompted the acceleration of scientific research in related fields. It is well known that there multiple solid–liquid two-phase interfaces occur during the BF ironmaking process. The solid and liquid phases undergo physical and chemical reactions at the interface, leading to the occurrence of element migration. The contact angle is an important parameter that reflects the wettability of a solid surface. By adjusting the contact angle between the two phases, not only is the consumption of refractories is reduced, but smooth operation of the BF and the quality of the hot metal are also ensured [18–20].

The results obtained from the literature regarding the erosion of slag and refractories are inconsistent because of different application backgrounds and experimental conditions. The effect of the corrosion behavior of the FeO–CaO–SiO₂–MgO–Al₂O₃ converter slag on Al₂O₃ substrate refractories was investigated by Song et al. [21]. The research results revealed that the sample was easily wetted with Al₂O₃ substrate when the temperature increased up to 1400 °C. The erosion process could be defined in terms of three main stages: melting, dissolution and diffusion, and cooling and crystallization. The erosion phenomenon was mainly attributed to the dissolution of Al³⁺ in the substrate into the slag. Sarkar et al. [22] discussed the interaction between FeO and alumina small plates under the condition of flash ironmaking. The results demonstrated that FeAl₂O₄ was found in the interface layer via XRD and SEM-EDS technology, and Fe²⁺ and Al³⁺ cations underwent reverse diffusion through the FeAl₂O₄ layer. The diffusion ability mainly depends on the temperature, and the effective diffusion coefficient (*D_{eff}*) and the average thickness of the spinel layer increased when the temperature rose. Wang et al. [23] examined the transient interaction between molten iron, the Al₂O₃ lining refractory, and the slag phase. The transient shape and thickness of the iron–slag–lining three-phase interface was measured and discussed by the authors. Their findings suggested that the erosion phenomenon was primarily caused by the molten iron entering the Al₂O₃ refractory. The reaction layer included two sub-layers: an Fe-rich layer adjacent to the iron with more FeO and less Al₂O₃, and an Al₂O₃-rich layer, which contained more Al₂O₃ and less FeO. FeO was generated due to the re-oxidation of molten iron, and entered the space between the refractory and molten iron. The thickness of the reaction layer increased approximately linearly with increasing time, indicating that the presence of FeO enhanced the erosion of molten iron on the lining refractory. In summary, despite significant previous research efforts regarding the erosion of the slag and Al₂O₃ refractory [24,25], there remains a scarcity of studies on the influence of *w*(FeO) in the BF primary slag containing FeO–CaO–SiO₂–MgO–Al₂O₃ on the erosion of Al₂O₃ substrate. Therefore, it is of great significance to investigate this issue.

In this context, the influence of *w*(FeO) in the BF primary slag containing FeO–CaO–SiO₂–MgO–Al₂O₃ on the erosion thickness of Al₂O₃ substrate was fundamentally investigated using the high-temperature contact angle method and FactSage thermodynamic software. The action mechanism of FeO on the interface between the slag and Al₂O₃ substrate was determined through the measurement of the observed contact angle and melting temperature during the wetting process, in addition to the line scanning results of SEM-EDS. The results of this study will provide guidance for reducing the consumption of refractory materials and effectively controlling the operating costs of the BF.

2. Materials and Methods

2.1. Materials

The composition of the mixed slag in the experiment was selected according to the composition of the BF primary slag of a local iron and steel enterprise, and was composed of analytical-grade pure reagents CaO, SiO₂, MgO, and Al₂O₃. The mass fractions of FeO in slags A and B were 10% and 15% respectively, and the basicity (C/S) was 1.4, as shown in Table 1. The pure oxides (CaO, SiO₂, MgO, and Al₂O₃) were thoroughly mixed in an agate mortar according to the predetermined proportion, then placed in a molybdenum crucible ($\varphi = 52 \text{ mm} \times H = 84 \text{ mm}$, 100 g), and calcined in a muffle furnace at 1500 °C for 6 h. During the calcination process, 1 L/min of high purity nitrogen (99.99%) was injected. The pre-melted slag was crushed and then ground in a ball mill machine for subsequent use. The commercially available ferrous oxalate dihydrate (FeC₂O₄·2H₂O) was placed in a molybdenum crucible, heated to 1000 °C, maintained at this temperature for 1 h, and then cooled to room temperature to obtain FeO powder. After drying, it was sealed and stored for later use or used immediately. Among the whole reaction process, 600 mL/min high purity nitrogen was continuously applied to prevent oxidation of FeO.

Table 1. Chemical composition of slags, wt%.

NO	C/S*	Slag Composition				
		FeO	CaO	SiO ₂	MgO	Al ₂ O ₃
Slag A	1.4	10	40.83	29.17	8	12
Slag B	1.4	15	37.92	27.08	8	12

C/S* = CaO (wt%)/SiO₂ (wt%).

A smooth surface was crucial for the accuracy of the wetting experiment. To obtain a smooth surface, the Al₂O₃ substrate was sanded using sandpaper of No. 800, 1000, and 1200 mesh in turn, polished with a polishing cloth, cleaned, and dried. The pre-melted slag and FeO powder were homogeneously mixed in a predetermined proportion (Table 1), and 0.8 g of the mixture was weighed using a high-precision electronic balance and then placed into a mold. The mixture was pressed for 3 minutes using a uniaxial hydraulic presser with a pressure of 10 MPa to obtain a cylindrical pellet ($\varphi = 8 \text{ mm} \times H = 6 \text{ mm}$). About 0.8 g of the mixture was placed on the Al₂O₃ substrate for the wetting experiment.

2.2. Experimental Setup and Methods

The wetting behavior of the slag and Al₂O₃ substrate was investigated using the high-temperature contact angle measurement instrument in the laboratory. A schematic diagram of the device is shown in Figure 1. The temperature was measured with a B-type thermocouple wrapped in alumina and placed near the sample, with an error of $\pm 2 \text{ K}$. The heating rate was 10 °C/min throughout the experiment. At the beginning of the experiment, the slag sample and Al₂O₃ substrate were first placed in the low-temperature zone of the furnace tube to prevent the sample from instantaneously breaking when contacting the high temperature, and then moved slowly to the high-temperature zone when the furnace temperature reached 1400 °C. High-purity nitrogen (1 L/min) was continuously injected throughout the experiment to prevent FeO from being oxidized at a high temperature. The drop image was continuously captured by a digital camera, and the contact angle between the slag droplets and the Al₂O₃ substrate was measured by the image processing software to determine the wettability of the slag and Al₂O₃ substrate.

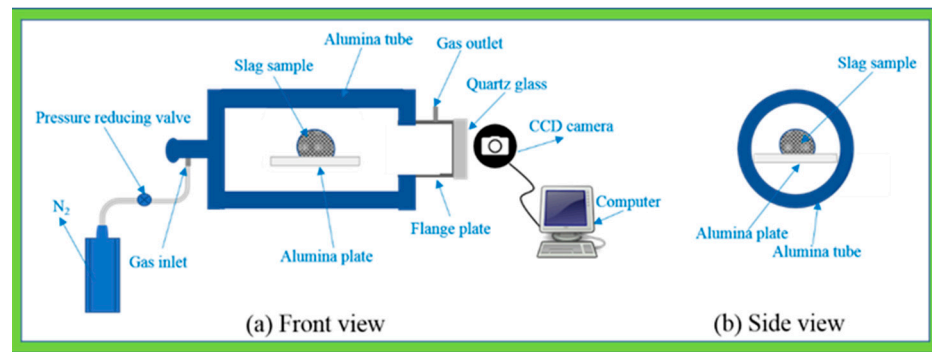


Figure 1. Schematic of experimental setup.

When the sample temperature reached 1400 °C, the sample was moved from the central high temperature zone of the furnace tube to the initial position, and the slag sample was quenched. To gain more insight into the mineral composition of the slag, some partially dried slag samples were analyzed by X-ray diffraction (XRD, Rigaku Ultima IV, Japan) under the following conditions: voltage: 40 mA; 40 kV; scanning range: 10–80° (2 θ); step size: 0.02° (2 θ); and scanning speed: 5°/min. The sample was embedded in epoxy resin and sliced so that the slag droplets and Al₂O₃ substrate were in the same horizontal plane. The treated sample surface was sanded using sandpaper (400, 800, 1000, 1200, and 1500 mesh in turn), and then polished, dried, and sprayed with gold. The cross-sectional microstructure and element distribution of the sample were analyzed by scanning electron microscopy coupled with energy-dispersive X-ray spectroscopy (SEM-EDS, sigma 500, Zeiss, Germany). The images were processed with Origin. The quinary equilibrium phase diagram of slag A (CaO-SiO₂-Al₂O₃-8 wt%MgO-10 wt%FeO) and the saturated solubility of Al₂O₃ in the liquid phase were calculated using FactSage 7.3 thermodynamic simulation software at 1400 °C and 1 atmospheric pressure (1 atm).

3. Results and Discussion

3.1. Wetting Behavior of Slag and Al₂O₃ Substrate

Figure 2 presents the schematic profiles of slags A and B droplets on the Al₂O₃ substrate at different temperatures. The start melting temperature, hemisphere point temperature, and complete melting temperature of the sample correspond to 5/6 H, 1/2 H, and 1/3 H (H—height of slag sample at 1100 °C), respectively, of the initial height of the sample [26,27]. It can be observed from the figure that the height of the slag samples decreases significantly with increasing temperature, which indicates that both types of slag diffuse rapidly along the Al₂O₃ substrate. When the slag sample reached 1400 °C, the contact angles θ_1 and θ_2 between the slag and Al₂O₃ substrate in Figure 2e were measured, and the arithmetic mean of the contact angles was defined as the observed contact angle θ , as shown in Equation (1).

$$\theta = (\theta_1 + \theta_2)/2 \quad (1)$$

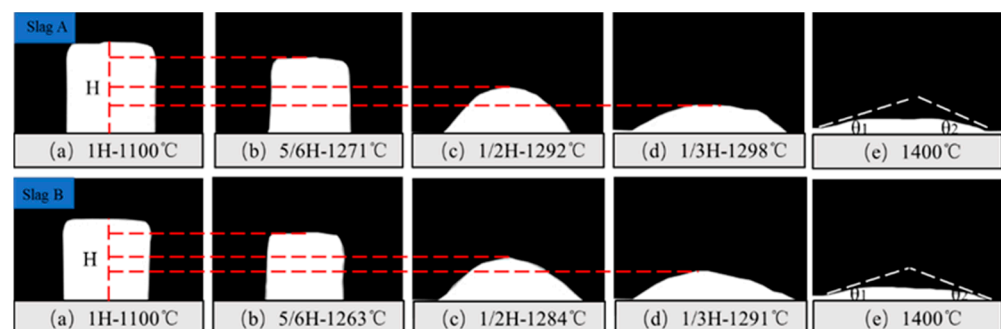


Figure 2. Schematic profiles of slag at different temperatures.

For primary slag with 10% and 15% FeO, the observed contact angles at 1400 °C were approximately 24.5° and 22°, respectively, indicating that slags A and B had better wettability with the Al₂O₃ substrate at this temperature. The better wettability may aggravate the erosion by slag of the Al₂O₃ refractory materials due to the interaction with the interface.

3.2. Effect of $w(\text{FeO})$ on Melting Temperature

The experimental results regarding the melting temperature of slag samples at different $w(\text{FeO})$ are shown in Figure 3. The starting melting temperature, hemispherical temperature, and complete melting temperature of the slag samples decrease as $w(\text{FeO})$ increases from 10% to 15%. The starting melting temperature is reduced from 1271 to 1263 °C. As a consequence of the melting point of FeO (1370 °C) being lower than that of the other oxides in the slag system, more FeO reacts with SiO₂ to form increasingly complex low-melting point compounds, such as FeO·SiO₂, thereby reducing the melting temperature of the slag. Figure 2 shows the lower temperature corresponding to the slag with high $w(\text{FeO})$ under the same proportion of the residual height ratio. Li et al. [28] studied the influence of $w(\text{FeO})$ on the melting characteristics of the primary slag under various slag basicity values. The results revealed that the melting temperature of the primary slag is significantly influenced by $w(\text{FeO})$ regardless of the slag basicity. Moreover, the melting temperature of the primary slag significantly declines with the increase in $w(\text{FeO})$. It can be seen from the above that the research results also show this trend.

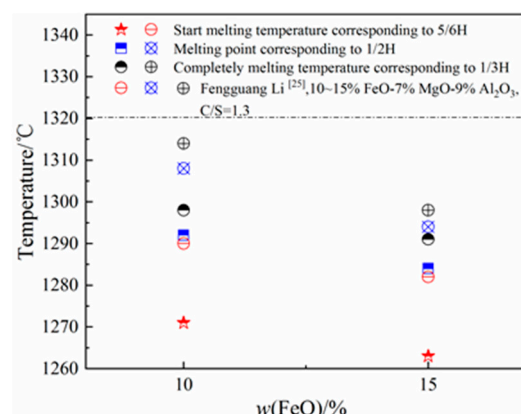


Figure 3. Starting melting temperature, hemisphere point temperature, and complete melting temperature of the sample at different $w(\text{FeO})$.

3.3. Mineral Composition of Slags

To further understand the mineral composition of the slag with different $w(\text{FeO})$, the samples of slags A and B were characterized by power XRD. The XRD pattern in Figure 4 shows the mineral composition of slags A and B. The obvious irregular diffraction peaks are mainly caused by the rapid cooling after the wetting experiment. According to the figure, the mineral phases formed in slags A and B are essentially identical, and mainly include akermanite (Ca₂MgSi₂O₇), gehlenite (Ca₂Al₂SiO₇), merwinite (Ca₃MgSi₂O₈), fayalite (Fe₂SiO₄), dicalcium silicate (Ca₂SiO₄), and (Mg, Fe) O. The results show that slag B contains more Fe₂SiO₄ and (Mg, Fe) O than slag A, which is likely due to the higher $w(\text{FeO})$. More Fe₂SiO₄ phase is the main reason for the decrease in the melting temperature in the previous section. In the current study, because the interface layer is very narrow and difficult to separate from the substrate, the XRD patterns show the mineral composition without the interface layer. The chemical composition of the interface layer is analyzed and discussed according to the quinary equilibrium phase diagram in Section 3.6.2.

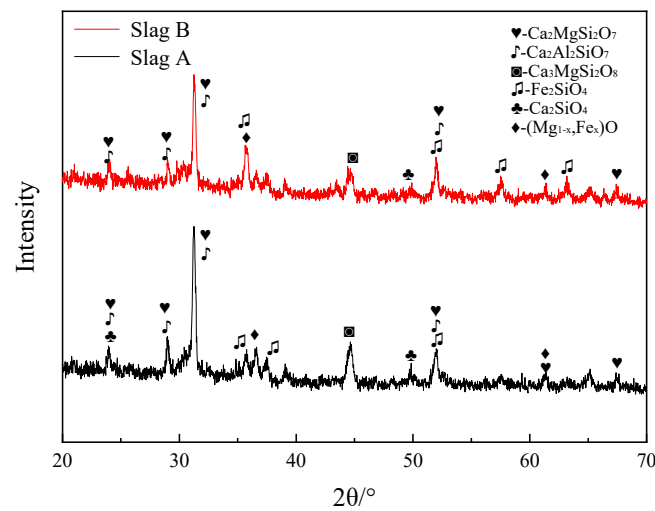


Figure 4. Mineral composition of slag with different $w(\text{FeO})$ at 1400 °C.

3.4. Element Distribution and Microstructure

The microstructure and elemental composition in the cross-section of the slag and Al_2O_3 substrate after the wetting experiment were analyzed using SEM-EDS, and the mapping results are visualized in Figures 5 and 6. The graphs indicate that the microstructure and element distribution of slags A and B are approximately the same, and the main elements include Fe, Ca, Si, Mg, Al, and O. The cross-section is mainly composed of a uniform gray phase area, a bright phase area, and a small dark gray phase area. The results of the energy spectrum at different positions of slags A and B are presented in Table 2. The dark gray area contains a large quantity of Al_2O_3 and CaO, in addition to a trace amount of SiO_2 , which corresponds with the results achieved by scanning shown in Figures 5 and 6. It is speculated that there is $\text{Ca}_2\text{Al}_2\text{SiO}_7$ in calcium aluminosilicate minerals. It is also noted that, for the gray phase area, the composition proportions of CaO, MgO, Al_2O_3 , and SiO_2 are close to those of the original slag, which is a homogeneous liquid phase formed at a high temperature. Moreover, the relative mass percentage of FeO in slag B is higher than that in slag A, which coincides with the experimental proportion of FeO in Table 1. The bright phase area mainly contains FeO and MgO. Combined with the scanning results of Figures 5 and 6, it can be seen that there are more Mg elements in the Fe-rich region, which is a continuous solid solution of (Mg, Fe) O. This is because Mg^{2+} in MgO can partially replace the vacancy of Fe^{2+} in the FeO crystal lattice and form (Mg, Fe) O solid solution. Moreover, the amount of solid solution increases with the increase in $w(\text{FeO})$, which can lead to the grains aggregating in pieces. This is consistent with the above-mentioned mapping results.

Table 2. EDS composition at different locations.

NO _i	Locations	Composition (wt%)				
		FeO	CaO	SiO ₂	MgO	Al ₂ O ₃
Slag A	Light	77.65	1.04	0.15	9.56	11.60
	Grey	4.42	40.19	36.43	7.90	11.06
	Dark grey	3.30	34.01	14.64	2.29	45.76
Slag B	Light	71.75	1.89	1.62	11.78	12.96
	Grey	5.92	40.67	34.46	6.76	12.19
	Dark grey	3.63	30.74	17.25	0.56	47.82

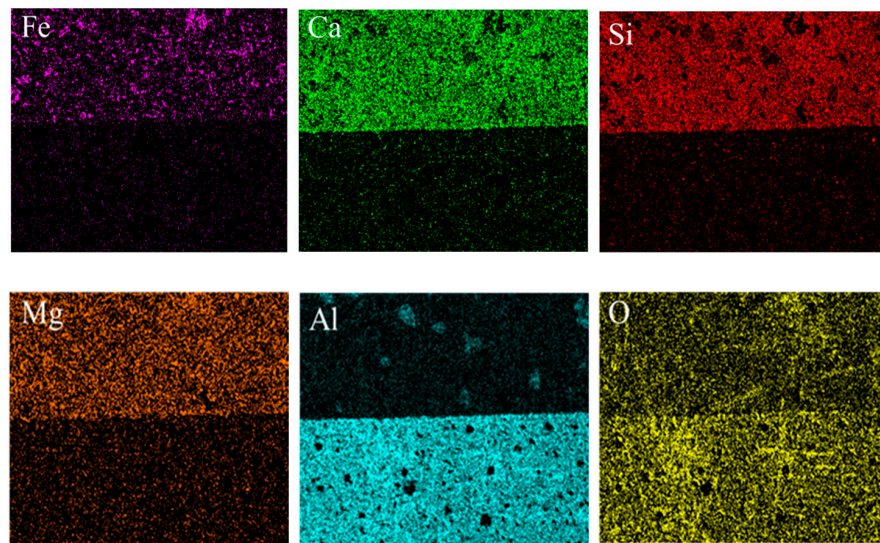
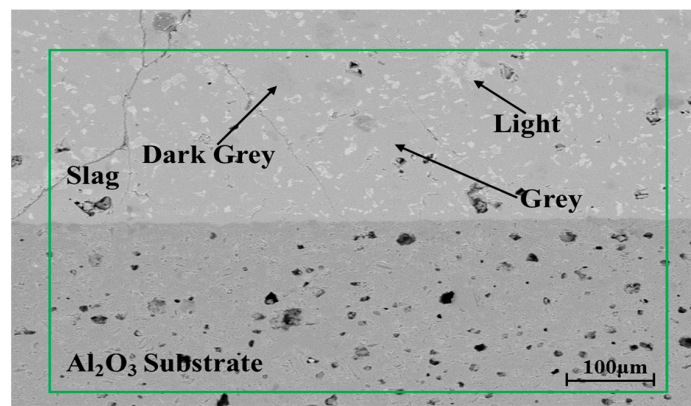


Figure 5. Element distribution of slag A.

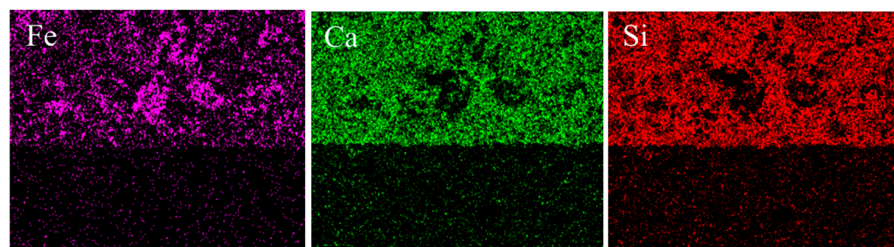
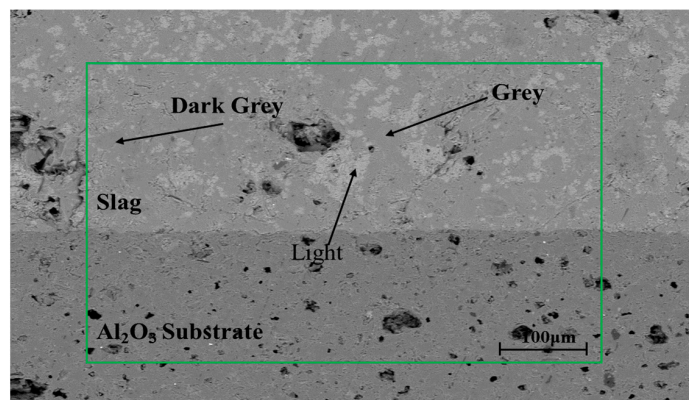


Figure 6. Cont.

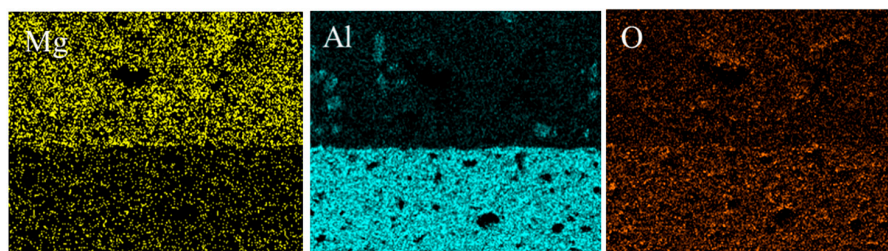


Figure 6. Element distribution of slag B.

3.5. Erosion Thickness of Slag and Al_2O_3 Substrate

Based on the SEM-EDS analysis, the influence of the slag on the erosion thickness of the Al_2O_3 substrate after the wetting experiment was studied. The line scanning results of slags A and B in different regions are shown in Figures 7 and 8, respectively. At high-temperature conditions, Al_2O_3 will dissolve into the slag, and different Al element content gradients form an interface layer. In the distance range of 0–250 μm , the average Al content in the slag is taken as the reference and the parallel line with the X axis is called the “average baseline” (see Figure 7b (Al) and Figure 8b (Al)). This intersects with the gradually increasing Al content change curve, and the vertical line between the intersection point and the X axis is defined as the starting position of erosion. Because the Al_2O_3 substrate contains almost no elements such as Fe, Ca, and Si, the vertical line between the point at which the element content approaches 0 and the X axis is the end position of erosion. The distance between the two vertical lines is regarded as the thickness of the interface layer. Because the diffusion rates of elements are not comparable, the measurement errors can be reduced to the maximum extent based on the average value of Al content. According to Figures 7b and 8b, the cross-section is largely categorized into three layers: the sample layer (layer I), the interface layer (layer II), and the original Al_2O_3 substrate layer (layer III). Within layer II, Ca content in slags A and B increases first and then tends to decrease, indicating that the Ca element diffuses into the interface layer. Moreover, it can also be observed that the content of the Fe element in slag A decreases gradually, whereas the same element in slag B initially increases and then decreases, and the content of Fe in slag B is relatively higher. The above-mentioned phenomena are caused by two possible factors: one is that the $w(FeO)$ in slag B is higher than that in slag A; the other is that there are some Fe-rich regions above the slag B interface layer, which leads to the migration of the Fe element to the interface layer. The thickness of the interface layer of slags A and B can be observed to be 19.23 and 23.17 μm , respectively, indicating that increasing the $w(FeO)$ in the slag can increase the thickness of the interface layer.

The chemical compositions of energy spectrum analysis results in different regions are presented in Table 3. It can be observed that the composition of the oxide corresponding to the weight percentage of spot 1 (layer I) in Figures 7 and 8 is close to that of the original slag. According to the results of Section 3.3, the slag may be composed of $Ca_2MgSi_2O_7$, $Ca_2Al_2SiO_7$, $Ca_3MgSi_2O_8$, Fe_2SiO_4 , Ca_2SiO_4 , and (Mg, Fe) O. The chemical composition of spot 2 (layer II) in the figure is mainly composed of Al_2O_3 , CaO, and SiO_2 . As the $w(FeO)$ in the slag increases from 10% to 15%, the values of $FeO/(Al_2O_3+CaO+SiO_2+MgO)$ in the interface layer of slags A and B are 0.073 and 0.123, respectively. It can be clearly observed that the value of slag A is relatively low. Moreover, FeO easily reacts with SiO_2 to generate a low-melting-point Fe_2SiO_4 , which has good fluidity and is interpenetrated with the generated high-melting-point slag. It can act as a cosolvent and increase the diffusion of Al_2O_3 to the interface layer, so the slag containing more FeO can aggravate the erosion thickness on the Al_2O_3 substrate.

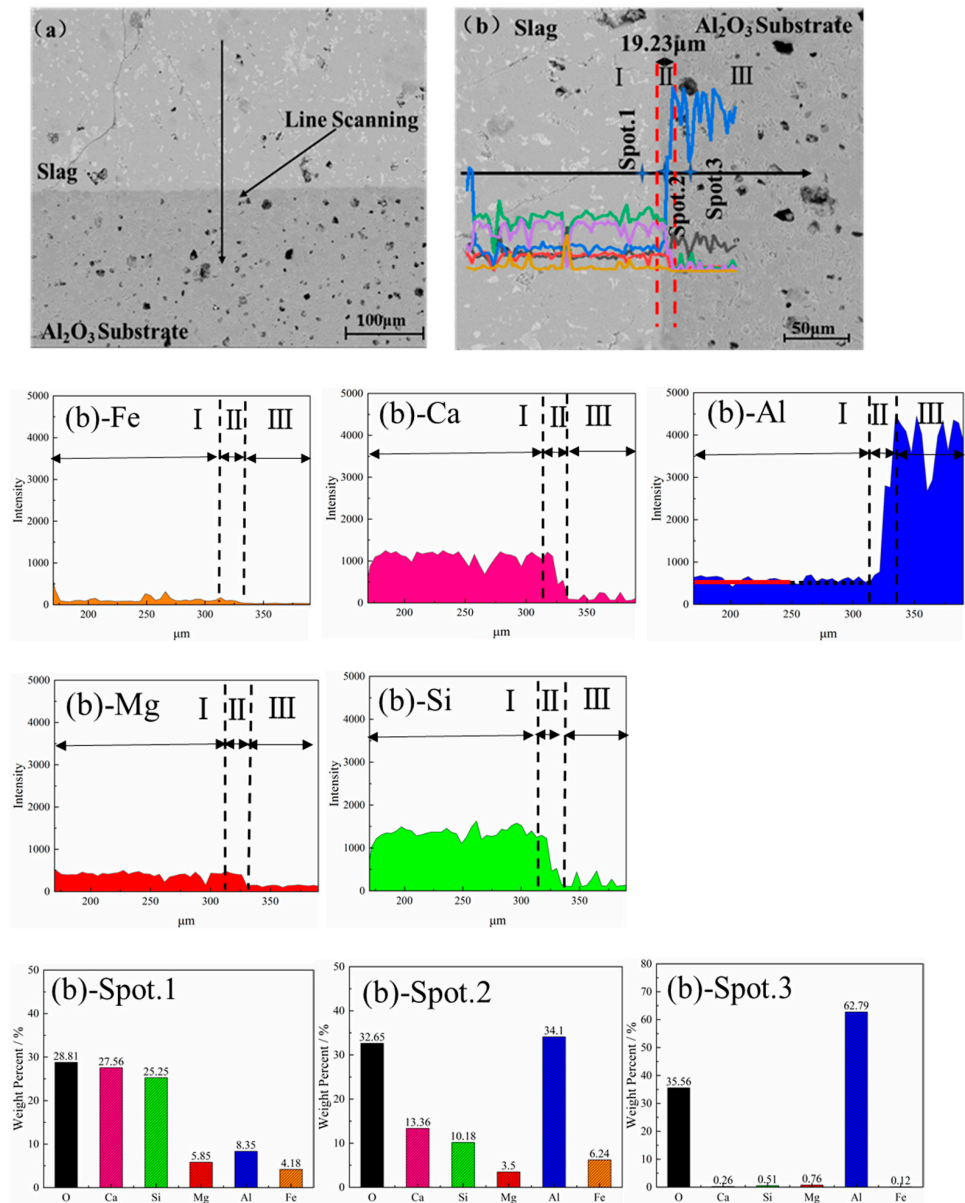


Figure 7. Line scanning results of slag A.

Table 3. EDS composition at different locations.

NOi	Locations	Composition/(wt%)				
		FeO	CaO	SiO ₂	MgO	Al ₂ O ₃
Slag A	Spot.1	4.35	31.22	43.78	7.89	12.76
	Spot.2	6.76	15.75	18.36	4.91	54.22
	Spot.3	0.14	0.29	0.90	1.04	97.63
Slag B	Spot.1	5.79	35.04	40.65	6.41	12.11
	Spot.2	10.96	9.25	18.73	6.16	54.90
	Spot.3	0.22	0.91	2.20	1.48	95.19

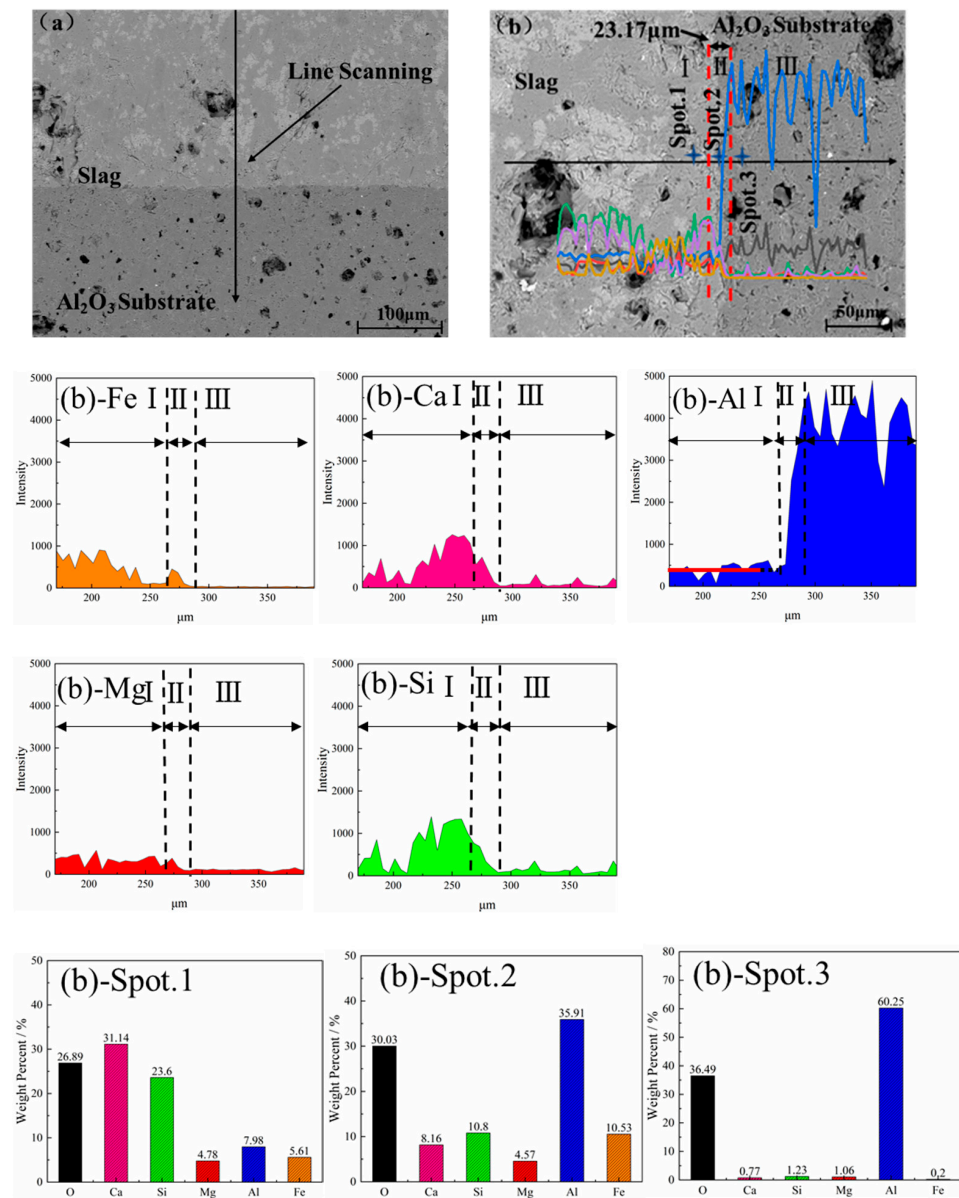


Figure 8. Line scanning results of slag B.

3.6. Corrosion Mechanism

3.6.1. Solubility of Al_2O_3 in the Liquid Phase

According to Figure 7b (Al) and Figure 8b (Al), there is a significant difference in Al content between layers I and II, which is mainly because the Al_2O_3 in the substrate continuously dissolves into the slag. The saturation solubility of Al_2O_3 in the particular sample was calculated using FactSage 7.3 (1400 °C, 1 atm), and the curves are demonstrated in Figure 9. The presented graph indicates that the content of Al_2O_3 in the liquid phase first shows an increasing trend and then decreases with a higher Al_2O_3 content. When the slag contains 27% Al_2O_3 , the maximum saturation of Al_2O_3 in the liquid phase is found to be relatively high, up to 21.21% and 26.15%, respectively. The content of Al_2O_3 in the original slag samples is 12%. From Figure 9, it can be observed that the content of Al_2O_3 in slags A and B does not reach saturation, which illustrates that Al_2O_3 dissolves and migrates to the slag.

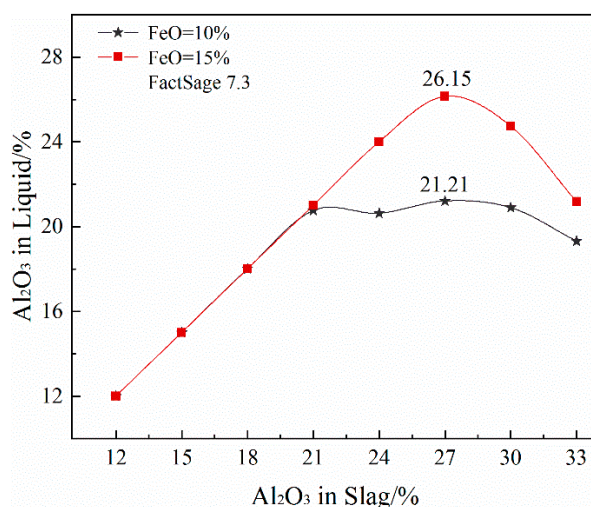


Figure 9. The solubility of Al₂O₃ in liquid phase.

3.6.2. Crystallization Process of the Interface Layer

When the temperature reached 1400 °C, the rapid cooling was carried out, and the crystallization process of layer II can be explained by the quinary phase diagram in Figure 10. The point “O” in Figure 10 is the original composition of slag A and is located in the primary crystal region of Ca₃MgSi₂O₈. We hypothesize that the dissolution of Al₂O₃ into the slag at a high temperature only changes the chemical composition of the interface layer, and the composition of the slag will move along a straight line in the O→N direction. This component point transfers to the primary crystal region of Ca₂Al₂SiO₇ or CaMg₂Al₁₆O₂₇, and Ca₂Al₂SiO₇ and CaMg₂Al₁₆O₂₇ phases with a high melting temperature will be generated in the interface layer after cooling. As can be seen from the mass percentage of the energy spectrum in Figures 7 and 8, at point 2, the interface layer mainly consists of Ca, Si, and Al elements, in addition to a small amount of Mg and Fe. The results demonstrate that Ca and Si diffuse to the interface layer and Al₂O₃ substrate dissolves into the slag during wetting. Sarkar et al. [29] discussed the interaction of Al₂O₃ refractories with FeO-SiO₂ and FeO-SiO₂-CaO slag, and found that the effective diffusion coefficients of Fe²⁺ and Al³⁺ were reduced significantly due to the formation of high-melting-point compounds, such as hercynite (FeAl₂O₄), mullite (3Al₂O₃·2SiO₂), and anorthite (CaAl₂Si₂O₈), in the interface layer, indicating that the high-melting-point compounds may further inhibit the diffusion of Al³⁺ ion into the slag. According to our experimental results, the Ca₂Al₂SiO₇ and CaMg₂Al₁₆O₂₇ phases can hinder the diffusion of Al³⁺.

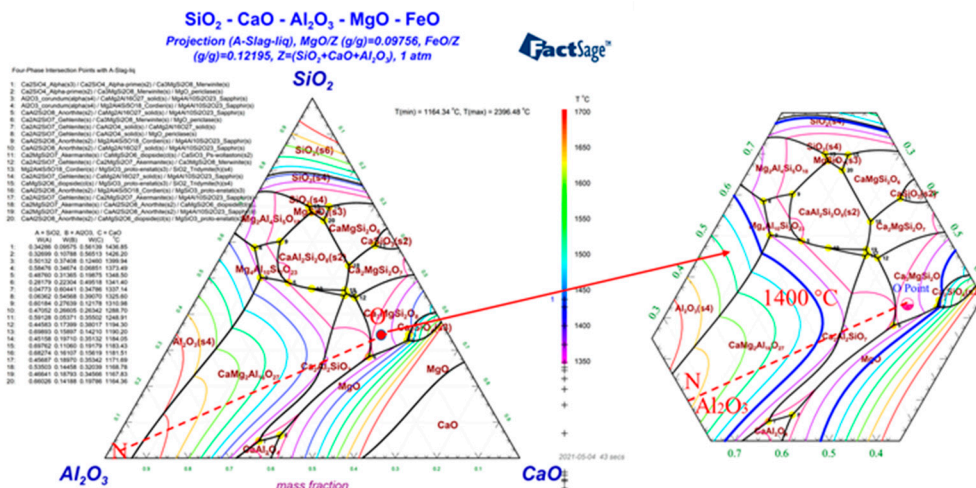


Figure 10. CaO-SiO₂-Al₂O₃-8% MgO-10% FeO quinary phase diagram.

In summary, the erosion mechanism of slag on Al_2O_3 substrate can be explained by the schematic diagram in Figure 11. Upon heating, the proportion of residual height of the solid slag decreases and gradually fuses into a liquid state. The good wettability of molten slag and Al_2O_3 substrate is the first step leading to substrate erosion as the temperature reaches $1400\text{ }^\circ\text{C}$. Furthermore, the dissolution of Al_2O_3 in the substrate into the slag is another significant factor of substrate erosion. The line scanning results in Figures 7 and 8 also prove the distribution of Ca, Si, and Al elements from the slag layer to the substrate layer. With the dissolution of Al_2O_3 and the interaction between CaO , MgO , SiO_2 , and Al_2O_3 , the phase with a high melting temperature precipitates at the interface layer. Moreover, a higher amount of FeO can easily generate a higher number of low-melting-point compounds with SiO_2 and coexist with high-melting-point slag, which increases the diffusion of Al_2O_3 and leads to the increase in erosion thickness. By comparison, the high-melting-point products are gradually covered between the slag and the Al_2O_3 substrate, which further represses the dissolution of Al_2O_3 . Based on the points discussed above, it can be concluded that a lower $w(\text{FeO})$ can reduce the erosion degree of slag on the Al_2O_3 substrate.

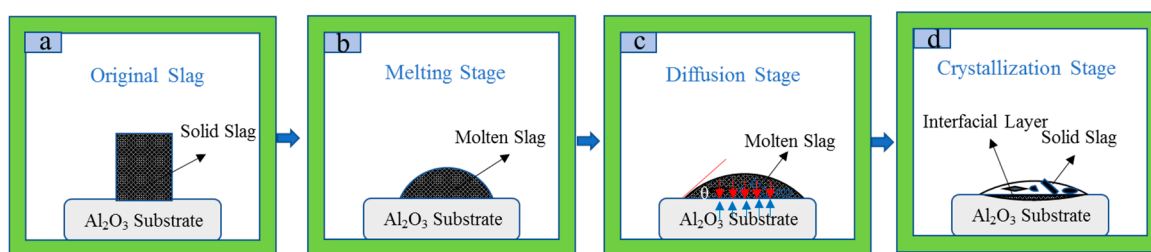


Figure 11. The schematic diagram of erosion mechanism.

4. Discussion

The effect of the erosion behavior of BF primary slag containing FeO - CaO - SiO_2 - MgO - Al_2O_3 on Al_2O_3 substrate was investigated using the high-temperature contact angle method and FactSage thermodynamic software. The main results are presented below.

(1) For primary slag with 10% and 15% FeO , the observed contact angles at $1400\text{ }^\circ\text{C}$ were approximately 24.5° and 22° , respectively, indicating that slags A and B had good wettability with the Al_2O_3 substrate. Moreover, the starting melting temperature of slag with 15% FeO , of $1263\text{ }^\circ\text{C}$, was lower.

(2) The mineral phases formed in slags A and B were essentially identical, and more Fe_2SiO_4 was observed in slag B. The thickness of the interfacial layer of slags A and B was found to be 19.23 and $23.17\text{ }\mu\text{m}$, respectively, indicating that a higher FeO in the slag can aggravate the erosion degree of Al_2O_3 substrate.

(3) Good wettability and dissolution of Al_2O_3 into slag are two important factors leading to substrate erosion. In addition, the formation of high-melting-point products can further inhibit the dissolution of Al_2O_3 substrate.

Author Contributions: Data curation, X.J.; methodology, X.P.; project administration, F.S.; software, H.Z.; writing—original draft, X.P.; writing—review & editing, Q.G. All authors have read and agreed to the published version of the manuscript.

Funding: This paper was financially supported by the National Science Foundation of China (51974073 and 52074086), the Foundational Research Funds of Zhongye Changtian International Engineering CO., LTD., China (2020JCYJ03), the Liaoning Provincial Natural Science Foundation of China (2019-MS-132), and the Fundamental Research Funds for the Central Universities, China (N2125029).

Institutional Review Board Statement: Not applicable.

Informed Consent Statement: Not applicable.

Data Availability Statement: Data sharing not applicable.

Conflicts of Interest: The authors declare no conflict of interest.

References

1. Jang, K.O.; Ma, X.; Zhu, J.; Xu, H.; Wang, G.; Zhao, B. Phase equilibria in the system CaO-SiO₂-Al₂O₃-MgO-15 and 20wt% “FeO” with CaO/SiO₂ ratio of 1.3. *ISIJ Int.* **2016**, *56*, 1728–1737. [[CrossRef](#)]
2. Eriksson, G.; Pelton, A. Critical evaluation and optimization of the thermodynamic properties and phase diagrams of the CaO-Al₂O₃, Al₂O₃-SiO₂, and CaO-Al₂O₃-SiO₂ systems. *Metal. Trans. B* **1993**, *24*, 807–816. [[CrossRef](#)]
3. Mao, H.; Hillert, M.; Selleby, M.; Sundman, B. Thermodynamic assessment of the CaO-Al₂O₃-SiO₂ system. *J. Am. Ceram. Soc.* **2006**, *89*, 298–308. [[CrossRef](#)]
4. Diaz, L.; Torrecillas, R.; Aza, A.; Pena, P. Effect of spinel Content on slag attack resistance of high alumina refractory castables. *J. Eur. Ceram. Soc.* **2007**, *27*, 4623–4631. [[CrossRef](#)]
5. Yi, S. Bosh slag chemistry control for high PCR and low slag volume blast furnace operation. *Steel Res. Int.* **2003**, *74*, 413–417. [[CrossRef](#)]
6. Jiao, K.; Zhang, J.; Chen, C.; Liu, Y. Effect of TiO₂ and FeO on the Viscosity and Structure of Blast Furnace Primary Slags. *Steel Res. Int.* **2017**, *88*, 1600296. [[CrossRef](#)]
7. Ma, X.; Zhao, B.; Zhang, D.; Zhi, X.; Evans, T. Phase Equilibria Studies in the CaO-SiO₂-Al₂O₃-MgO System with CaO/SiO₂ Ratio of 1.10. *ISIJ Int.* **2016**, *56*, 513–519. [[CrossRef](#)]
8. Ma, X.; Wang, G.; Wu, S.; Zhu, J.; Zhao, B. Phase Equilibria in the CaO-SiO₂-Al₂O₃-MgO System with CaO/SiO₂ Ratio of 1.3 Relevant to Iron Blast Furnace Slags. *ISIJ Int.* **2015**, *55*, 2310–2317. [[CrossRef](#)]
9. Jang, K.O.; Ma, X.; Zhu, J.; Xu, H.; Wang, G.; Zhao, B. Phase Equilibria in the System “FeO”-CaO-SiO₂-Al₂O₃-MgO with CaO/SiO₂ 1.3. *ISIJ Int.* **2016**, *56*, 967–976. [[CrossRef](#)]
10. Ren, S.; Liu, Q.; Zhang, J.; Chen, M.; Ma, X.; Zhao, B. Laboratory study of phase transitions and mechanism of reduction of FeO from high Ti-bearing blast furnace primary slag by graphite. *Ironmak. Steelmak.* **2015**, *42*, 117–125. [[CrossRef](#)]
11. Pal, J.; Ghorai, S.; Goswami, M.; Ghosh, D.; Bandyopadhyay, D.; Ghosh, S. Behavior of fluxed lime iron oxide pellets in hot metal bath during melting and refining. *Int. J. Miner. Metall. Mater.* **2013**, *20*, 329–337. [[CrossRef](#)]
12. Zhang, Z.; Xu, H.; Wu, S.; Liu, Y. Effects of combined pre-straining and pre-aging on natural aging and bakehardening response of an Al-Mg-Si alloy. *Acta Metall. Sin.* **2013**, *26*, 340–344. [[CrossRef](#)]
13. Shen, F.; Jiang, X.; Wu, G.; Wei, G.; Li, X.; Shen, Y. Proper MgO Addition in Blast Furnace Operation. *ISIJ Int.* **2006**, *46*, 65–69. [[CrossRef](#)]
14. Wang, D.; Ma, K.; Xu, Y.; Xu, J.; Wen, L. *Influences of CaO/SiO₂/MgO/Al₂O₃ on the Formation Behavior of FeO-Bearing Primary-Slags in Blast Furnace*; Springer International Publishing: New York, NY, USA, 2017; pp. 251–258.
15. Sako, E.; Braulio, M.; Luz, A.; Zingrebe, E.; Pandolfelli, V. Slag resistance of Al₂O₃-MgO refractory castables in different environmental conditions. *J. Am. Ceram. Soc.* **2013**, *96*, 3252–3257. [[CrossRef](#)]
16. Blond, E.; Schmitt, N.; Hild, F.; Blumenfeld, P.; Poirier, J. Effect of slag impregnation on thermal degradations in refractories. *J. Am. Ceram. Soc.* **2007**, *90*, 154–162. [[CrossRef](#)]
17. Cheremisina, E.; Schenk, J.; Nocke, L.; Paul, A.; Wimmer, G. Kinetics and Mechanisms of Dolime Dissolution in Steelmaking Slag. *Metall. Mater. Trans. B* **2019**, *50*, 1269–1276. [[CrossRef](#)]
18. Cooper, A.R. Kinetics of refractory corrosion. In *Ceramic Engineering and Science Proceedings*; John Wiley & Sons Inc.: Hoboken, NJ, USA, 1981; pp. 1063–1089.
19. Afshar, S.; Allaire, C. The corrosion of refractory aggregates by molten aluminum. *JOM* **2000**, *52*, 43–46. [[CrossRef](#)]
20. Monaghan, B.; Abdeyazdan, H.; Dogan, N.; Rhamdhani, M.; Longbottom, R.; Chapman, M. Effect of slag composition on wettability of oxide inclusions. *ISIJ Int.* **2015**, *55*, 1834–1840. [[CrossRef](#)]
21. Song, J.; Liu, Y.; Lu, X.; You, Z. Corrosion behavior of Al₂O₃ substrate by SiO₂-MgO-FeO-CaO-Al₂O₃ slag. *J. Mater. Res. Technol.* **2019**, *9*, 314–321. [[CrossRef](#)]
22. Sarkar, R.; Sohn, H. Interaction of ferrous oxide with alumina refractory under flash ironmaking conditions. *Ceram. Int.* **2019**, *45*, 15417–15428. [[CrossRef](#)]
23. Chen, Y.; Wang, J.; Zhang, L. Transient interaction between molten iron, alumina lining refractory and slag. *J. Manuf. Sci. Prod.* **2013**, *13*, 133–143.
24. Choi, J.; Lee, H.; Kim, J. Dissolution rate of Al₂O₃ into molten CaO-SiO₂-Al₂O₃ slags. *ISIJ Int.* **2002**, *42*, 852–860. [[CrossRef](#)]
25. Choi, J.; Lee, H. Wetting of solid Al₂O₃ with molten CaO-Al₂O₃-SiO₂. *ISIJ Int.* **2003**, *43*, 1348–1355. [[CrossRef](#)]
26. Wang, H.; Li, G.; Ding, Z.; Dai, Q.; Li, B. Effect of additives on melting point of LATS refining ladle slag. *J. Iron Steel Res. Int.* **2007**, *14*, 25–29. [[CrossRef](#)]
27. Wang, H.; Li, G.; Li, B.; Zhang, X.; Yan, Y. Effect of B₂O₃ on melting temperature of CaO-based ladle refining slag. *J. Iron Steel Res. Int.* **2010**, *17*, 18–22. [[CrossRef](#)]
28. Li, F.; Qi, C.; Wang, Y. Effect of FeO on softening characteristics of primary slag under different alkalinity. *Iron Steel* **2018**, *53*, 26–32. (In Chinese)
29. Sarkar, R.; Hong, Y. Interaction of pure alumina refractory with FeO-SiO₂ and FeO-SiO₂-CaO slags relevant to the novel flash ironmaking technology. *Steel Res. Int.* **2019**, *90*, 1900104. [[CrossRef](#)]